Osmotic manipulation of particles for microfluidic applications

Benjamin Abécassis, Cécile Cottin-Bizonne, C. Ybert, A. Ajdari, L. Bocquet

New Journal of Physics
The open-access journal for physics

Osmotic manipulation of particles for microfluidic applications

B Abécassis[1,2], C Cottin-Bizonne[1], C Ybert[1], A Ajdari[2] and L Bocquet[1,3]

[1] Laboratories PMCN, Université Lyon 1; Université de Lyon, UMR CNRS 5586, 69622 Villeurbanne, France
[2] UMR CNRS Gulliver 7083, ESPCI, 75005 Paris, France
E-mail: lyderic.bocquet@univ-lyon1.fr

New Journal of Physics **11** (2009) 075022 (21pp)
Received 6 January 2009
Published 31 July 2009
Online at http://www.njp.org/
doi:10.1088/1367-2630/11/7/075022

Abstract. Diffusiophoresis, i.e. the movement of macromolecules along a molecular gradient, is shown to be an efficient means to drive particles in microchannels. By using a generic microfluidic setup, we assess the displacement of silica particles under a controlled salt gradient and provide experimental evidence for a strongly enhanced migration process, the amplitude of which depends on the nature of the salt. A theoretical description shows quantitative agreement with the observed experimental features. Furthermore, we describe a set of microfluidic operations such as separation, sorting or focusing of a colloidal assembly which can be efficiently performed using diffusiophoresis.

[3] Author to whom any correspondence should be addressed.

Contents

1. Introduction

During recent years, the pursuit of scale reduction inherent to nanotechnologies has been extended to the fluidic domain, with the very active development of microfluidics and now nanofluidics [1, 2]. Such microscale 'lab-on-a-chip' devices are already widely used in biotechnological applications for target screening, drug design and for the analysis of small probes of biological material. However, increasing the density of fluidic operations on a chip even further, i.e. miniaturizing fluidic devices more, leads to new questions and challenges, both from a fundamental and an application point of view. A key point is that future devices working at ever smaller scales cannot be thought on a basis of further scale reduction of existing devices working at larger scales: new solutions have to be found, taking the peculiarities of the small scales into account.

In this paper, we explore an alternative solution for particle manipulation in microfluidic systems, based on a solute-driven 'osmotic' mechanism, diffusiophoresis [3, 4]. Particle manipulation is indeed involved in many elementary operations in lab-on-a-chip processes, such as mixing, separation, fluid and particle induced motion, etc. Brownian motion and diffusive process are rather inefficient to drive colloidal particles on microscales and migration is most commonly induced under the application of external forces, such as gravity or electric fields [5]. Electrophoresis, i.e. motion induced by an electric field, belongs to the more general class of phoretic transport, that is, motion under the gradient of a field variable: an electric potential, temperature gradient, concentration of a chemical species, etc [4].

While electrophoresis is commonly used to manipulate charged colloids in microchannels [5], thermophoresis has been shown recently to allow for versatile driving, e.g. obtained by designing laser-induced temperature gradients [6]–[9].

Diffusiophoresis is an alternative—less explored—phoretic phenomenon, describing the motion of particles under the gradient of a solute, for example a salt [10]–[14]. In many aspects, diffusiophoresis resembles chemotaxis of cells and micro-organisms, i.e. motion towards higher concentrations of food or towards lower concentrations of poisons [15]. However, its origin is purely physical. Anticipating the discussions to follow in the paper, the origin of the diffusiophoretic motion is double. In the case of a binary electrolyte, two contributions can be distinguished. The first one is the *osmotic pressure gradient* induced by the solute gradient in the diffuse layer around the colloidal particles; a second, more obvious, contribution occurring in the case of diffusiophoresis induced by a salt gradient, is the electrophoresis induced by the *electric field created by the differential diffusional motion* of the electrolytes.

In contrast to electrophoresis, diffusiophoresis has received less attention in the perspective of lab-on-a-chip applications. It has several obvious advantages: it yields a potential means to convert chemical energy into directed motion; and in contrast to other phoretic mechanisms, it does not require an active external energy input, the size/weight of which can prevent its use in real portable lab-on-a-chip devices, here the only source of energy being a chemical internal gradient of a solute.

In a previous paper [16], we presented first results on the application of diffusiophoresis in colloid manipulation in microchannels. The present paper expands on this preceding study and provide furthermore a detailed theoretical framework describing the experimental results.

In particular, we show that diffusiophoresis can be used to efficiently drive colloidal particles in a microfluidic channel, by demonstrating both spreading and focusing of a colloidal assembly induced by a moderate salt gradient. Then, the proofs of principle for several elementary microfluidic operations (concentration, sorting, ...) are exhibited using this simple transduction mechanism.

2. Boosting migration using a fast carrier

2.1. Experimental setup and salt-induced migration

To achieve a systematic and quantitative analysis of the phenomenon, we study the migration of colloidal particles in a microfluidic device with a Ψ-channel geometry, schematized in figure 1(a). Two solutions are flowing alongside, one in the center of the channel and the other on its lateral sides. Unless otherwise stated, colloids (silica spheres of 200 nm in diameter at a concentration of 0.005% in mass) are injected in the central channel and all solutions have an equal speed, U. By adding salt to one of the solutions (central or lateral), a salt concentration gradient is achieved from the entrance of the channel. Such a microfluidic setup presents several advantages, which allow quantitative and fully reproducible results to be obtained, thus making it available for detailed comparisons with modelization. Indeed (i) it provides a stationary situation where time axis is read along the z-coordinate, defining an effective time $t = z/U$, with U the flow velocity; (ii) it allows one to generate and sustain a controlled solute gradient under stationary conditions; and (iii) it avoids unwanted convection effects. Particles are fluorescent silica colloids, with a diameter of 200 nm. Experimental methods and details are summarized in the appendix.

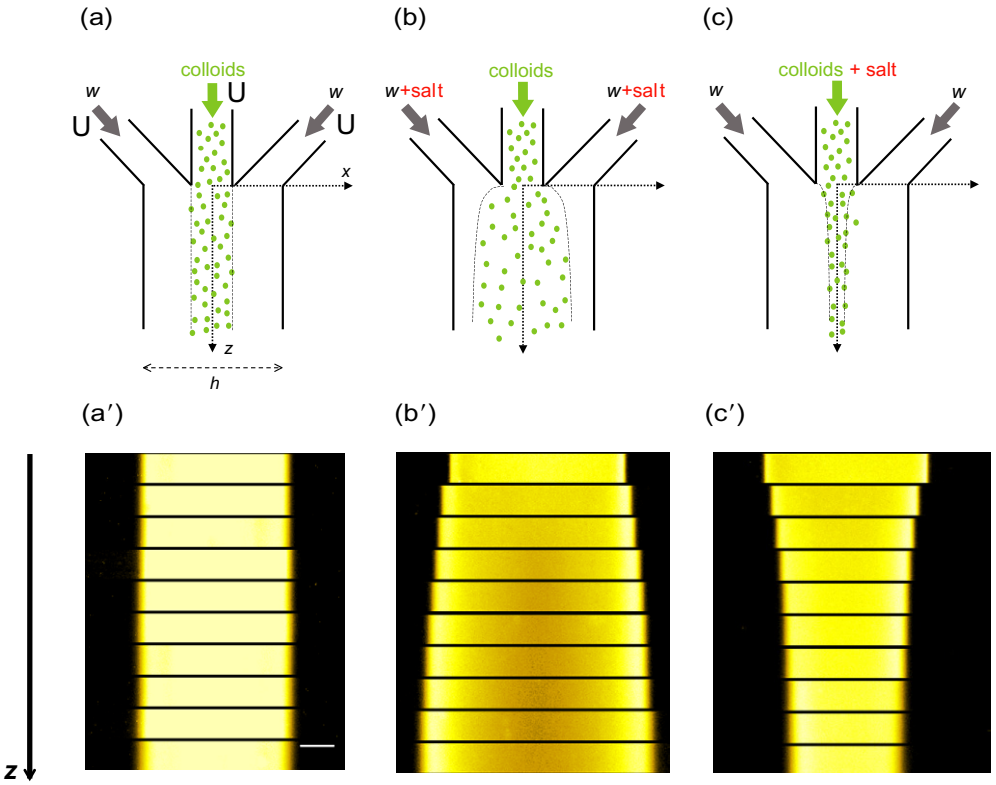

Figure 1. A solution of fluorescent colloids (mass fraction of 0.005% in colloids) is injected in the central inlet of a Ψ-shape microfluidic channel. Fluorescence images are acquired at different distances from the inlet. From top to bottom, the images correspond to the following z-distances: 0, 3, 7, 11, 14, 14.65, 23, 40, 50, 60, 84 mm. (a)–(a′): no salt is added to either of the solutions. 10 mM of LiCl is added either to the side streams ((b)–(b′)) or to the central stream ((c)–(c′)). The horizontal scale bar is 50 μm. As depicted in figure 1(a), the flow is along the direction z, whereas the salt gradient is along x; y is perpendicular to the plane of the figure (not shown). The width of the channel along x is h, whereas its thickness along y is y_0.

First, we show in figure 1(a)–(a′) the benchmark case of a pure buffer coflowing along the colloidal solution. In this case, there is no salt gradient and the only transport mechanism for the colloids is Brownian motion. As observed in figure 1(a′), no effect is observed in this case and the extension of the colloidal band remains constant from the beginning to the end of the channel (∼cm in length). Such behavior is actually expected since diffusion is inefficient to drive colloidal particles of this size at these time/length scales: this is quantified by an estimate of the 'mixing length' for the colloids, i.e. the length ℓ along the channel after which the colloids have explored the whole channel width due to diffusion. Typically $\ell = h^2 U / D_{\text{coll}} \approx 1$ m, which is two orders of magnitude larger than the actual channel length.

Now we turn to the demonstration of the diffusiophoretic effect. To this end, one adds 10 mM of a salt solution (LiCl) to the coflowing solution (figure 1(b)). As demonstrated in figure 1(b′), this small amount of salt induces a significant spreading of the colloidal band. On the other hand, focusing of the colloidal solution is observed when the salt is added to

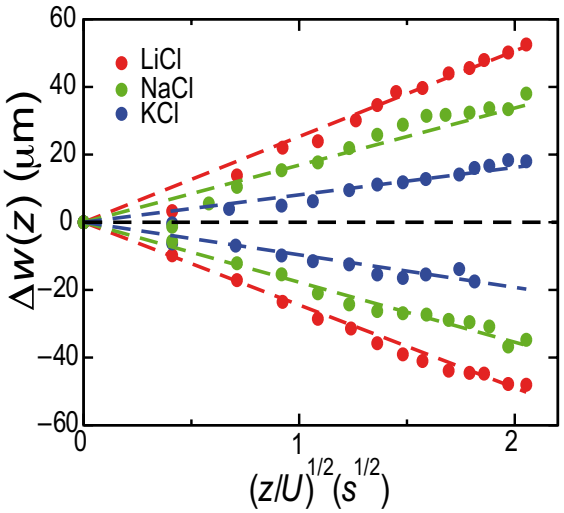

Figure 2. Width of the fluorescent band $\Delta w = w(z) - w_0$ as a function of the square root of the elapsed time ($t = z/U$) for the three salts considered (KCl, NaCl, LiCl), in the focusing ($\Delta w < 0$) and spreading ($\Delta w > 0$) configurations, corresponding respectively to figures 1(b) and 1(c).

the colloid branch, figure 1(c)–(c′). Colloid motion is therefore directed towards regions of higher salt concentration. Note that in both cases, the particle velocity is of the order of tens of micrometers per second.

2.2. A strongly enhanced migration

To quantify this behavior, we show in figure 2 the colloidal width, $\Delta w(z)$, versus the 'effective time' $t = z/U$ for three different salts (KCl, NaCl, LiCl). Both spreading $\Delta w > 0$ (for the geometry of figure 1(b)) and focusing $\Delta w < 0$ (for the geometry of figure 1(c)) occur for all the studied salts, but the amplitude of the effect is seen to be salt specific. The variation of the colloidal width on this timescale is proportional to $\sqrt{t}$, suggesting to introduce an effective diffusion coefficient D_{eff} according to

$$\Delta w(t) = \pm\sqrt{2D_{\text{eff}}t}, \tag{1}$$

the sign depending on the direction of the salt gradient.

The effective diffusion coefficient, normalized by the bare diffusion coefficient of the colloid, is plotted in figure 3 for the three salts studied, KCl, NaCl and LiCl. In the present situation, the effective diffusion coefficient is up to two orders of magnitude larger than D_{coll}, the bare diffusion coefficient of the colloids. We also note that the values obtained in the focus and spreading situations are very close to each other (thus suggesting a weak effect of the colloid concentration in our experiments).

This diffusive-like migration is, however, temporary and a saturation of the colloidal band occurs at long distances z, i.e. long effective times t. We plot in figure 4 the complete evolution of the colloidal band's width, $\Delta w(z) = |w(z) - w_0|$, as a function of the effective time $t = z/U$. Note that, as quoted above, the extension of the displacement is, within experimental uncertainty, the same for the focus and spreading configuration. At short times, the displacement

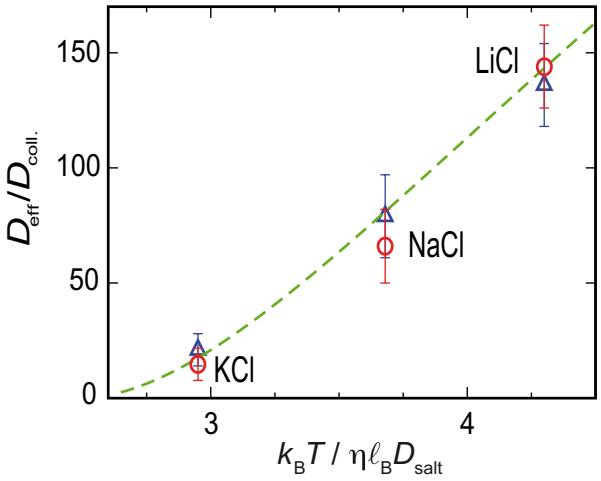

Figure 3. Effective diffusion coefficient, normalized by the bare colloid diffusion coefficient D_{coll} (blue triangles are for the focus situation and red circles are for the defocus geometry), as a function of the inverse normalized salt diffusivity, $k_{\mathrm{b}}T/\eta\ell_{\mathrm{b}}D_{\mathrm{s}}$ (D_{s} is the salt diffusion coefficient, η the water viscosity and $\ell_{\mathrm{b}} = 0.7\,\mathrm{nm}$ is the Bjerrum length). D_{coll} is calculated using the Stokes–Einstein relationship, $D_{\mathrm{coll}} = 2.18\,\mu\mathrm{m}^{-2}\,\mathrm{s}^{-1}$. The dashed line represents the theoretical prediction using equation (24), using the measured value of the ζ potential ($\zeta = -35 \pm 5\,\mathrm{mV}$) and $\alpha_{\mathrm{Pois}} = 1.8$.

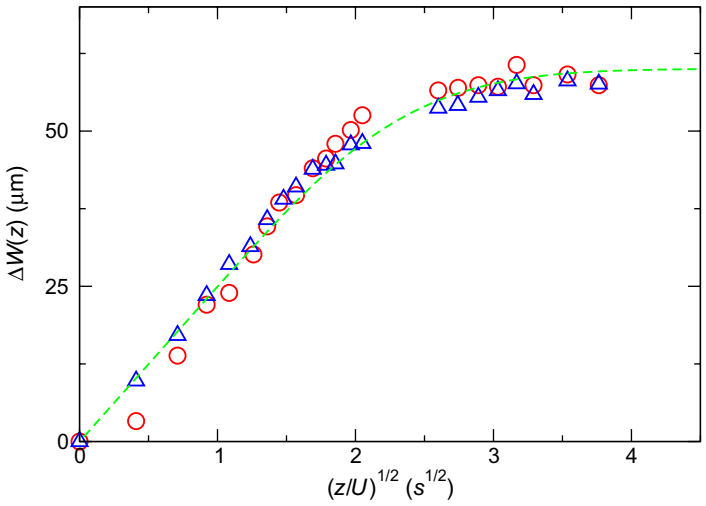

Figure 4. Evolution of the width of the colloid–water interface $|\Delta w(z)| = |w(z) - w(0)|$ versus $\sqrt{z/U}$ in the spreading (○) and focus (△) configurations. The salt is LiCl, with concentration 10 mM. The dashed line is the prediction of equation (18), using a zeta potential of the particles $\zeta = -35\,\mathrm{mV}$ and $\alpha_{\mathrm{Pois.}} = 1.8$.

of the colloid/water interface is linearly proportional to the square root of the effective time, as already discussed above. At longer times, the width of the colloidal band saturates at a stationary value, $\Delta w = \Delta w_{\infty}$. The origin of this saturation is quite clear: since salt contrast drives the colloidal migration, as we will detail in the next section, the saturation occurs in our geometry

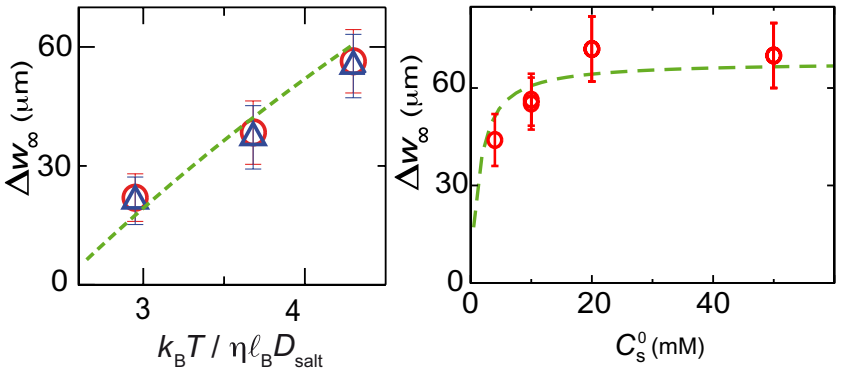

Figure 5. Left: saturation value of the width of the colloidal band versus the inverse normalized diffusivity of the salts. Blue triangles are for the focus situation and red circles are for the defocus geometry. Right: saturation value (for LiCl) as a function of salt concentration for the defocus situation, with respect to the buffer concentration (1 mM). Dashed lines represent theoretical predictions using equation (25), with parameters being the measured ζ potential (-35 mV) and $\alpha_{\mathrm{Pois}} = 1.8$.

due to the end of the salt diffusive process. This is expected to occur at a distance z of the order of the *salt mixing length*, $z \sim \ell_s = h^2 U / D_s$, with D_s the salt diffusion coefficient. Typically ℓ_s is of the order of centimeters here. We summarize in figure 5 the variations of Δw_∞ versus the salt nature (figure 5(a)) and salt concentration (figure 5(b)). We will come back to the theoretical predictions in the next section.

To conclude on the experimental results, we have shown that a contrast of salt concentration considerably enhances the migration of the colloidal particles. In our geometry, this enhancement is characterized by an effective diffusion coefficient which is up to two orders of magnitude larger than the bare diffusion coefficient. However, although the analogy to diffusive transport is appealing, this process differs from classical diffusion in several aspects. Firstly, both positive and negative diffusive-like migrations can be obtained in the present case, with a sign depending on the underlying salt gradient direction. Secondly, in a real diffusion process, the width of the colloid density profiles would spread diffusively towards a Gaussian, in contrast to the present situation (see, for example, the sharp colloid profiles in figures 1 and 7). Finally, at longer times, the width $w(z)$ is observed to saturate. The transport is therefore not diffusive, but deterministic, as we now discuss in detail.

3. Theoretical description of diffusiophoretic dynamics, results and discussion

The colloid migration observed in the above experiments can be attributed to diffusiophoresis, i.e. motion induced by a solute concentration gradient. We now develop a theoretical description of the effect.

3.1. Diffusiophoresis of the macromolecules

The diffusiophoretic velocity V_{DP} of the colloid is, for a binary electrolyte, linearly related to the salt concentration gradient ∇C_s according to [4]:

$$\mathbf{V}_{\mathrm{DP}} = D_{\mathrm{DP}} \cdot \nabla \log C_s. \tag{2}$$

The diffusiophoretic mobility, D_{DP}, has the dimension of a diffusion coefficient and has been calculated by Prieve and Roman in the case of charged particles and $z:z$ electrolyte. It takes the form [12]:

$$D_{\mathrm{DP}} = \frac{k_{\mathrm{B}}T}{\eta}\frac{\left[-\log(1-\gamma^2)+(1/2)\beta\Psi\right]}{2\pi\ell_{\mathrm{B}}}, \tag{3}$$

where $\Psi = z_0 e\zeta/k_{\mathrm{B}}T$ is the normalized zeta potential (ζ), $\gamma = \tanh(\Psi/4)$ and $\ell_{\mathrm{B}} = (z_0 e)^2/4\pi\epsilon k_{\mathrm{B}}T$ the Bjerrum length (e the unit charge, z_0 the valence of the ions and ϵ the dielectric constant of water). The (ion specific) factor β is defined in terms of the difference in diffusion constants of cations and anions: $\beta = (D_+ - D_-)/(D_+ + D_-)$.

As quoted earlier this expression has two contributions. The first term in equation (3) originates from the osmotic pressure gradient occurring within the Debye layer at the surface of the colloids. This pressure gradient is balanced by the viscous stress within the interfacial double layer, thereby inducing a fluid flow from the higher to lower salt concentration regions. Physically this can be expressed as:

$$\frac{\eta V_{\mathrm{DP}}}{\lambda_{\mathrm{D}}} \approx \lambda_{\mathrm{D}}\nabla[k_{\mathrm{B}}T C_{\mathrm{s}}] \tag{4}$$

with η the shear viscosity of water, λ_{D} the thickness of the Debye layer. Using $\lambda_{\mathrm{D}}^{-2} = 8\pi\ell_{\mathrm{B}}C_{\mathrm{s}}$ (ℓ_{B} the Bjerrum length, $\ell_{\mathrm{B}} = 0.7$ nm) [17], this predicts the salt-induced migration in equation (2), moreover with the expression $D_{\mathrm{DP}} \sim \frac{k_{\mathrm{B}}T}{\eta\ell_{\mathrm{B}}}$ in qualitative agreement with equation (3).

This contribution is often coined as 'chemiphoretic' as opposed to the electrophoretic effect which accounts for the second term of equation (3). As the cation and the anion of the salt have different diffusivities ($D_+ \neq D_-$), they will migrate at different speeds when a salt gradient is set up. For electroneutrality to be conserved, a macroscopic electric field emerges which slows down fast ions and accelerates slow ions [12]

$$E_{\mathrm{ind}} = \frac{k_{\mathrm{B}}T}{z_0 e}\beta\nabla\log C_{\mathrm{s}}. \tag{5}$$

This electric field originating in the salt gradient thus induces electrophoretic motion of the charged colloids. It derives from the so-called 'junction potential' which has been measured in microfluidic setups [18] and used to manipulate proteins [19]. In our geometry this electric field is typically of the order of a few hundreds of volts per meter (and maximum in the regions of strong salt gradient).

Both contributions ('chemiphoretic' and electrophoretic) are typically of the same order of magnitude. For KCl ($D_+ \simeq D_-$) only the 'chemiphoretic' contribution will persist whereas both effects will be present for NaCl and LiCl. The colloid migration is thus slaved to the salt dynamics, which we discuss now.

3.2. Diffusive dynamics of the salt

In general, the stationary salt concentration $C_{\mathrm{s}}(x, y, z)$ obeys a convection–diffusion equation:

$$v_z\frac{\partial}{\partial z}C_{\mathrm{s}}(x, y, z) = D_{\mathrm{s}}\Delta C_{\mathrm{s}}(x, y, z), \tag{6}$$

with Δ the usual Laplacian and v_z the imposed fluid flow field along the direction z. In the direction y (perpendicular to x and z, see figure 1), the flow takes the form of a parabolic Poiseuille profile, with a mean U: $v_z(y) = \frac{3}{2}U(1-(\frac{2y}{y_0})^2)$.

Let us note that the 'average' salt diffusion coefficient is defined in terms of $D_\pm$ according to $D_s = 2D_+D_-/(D_+ + D_-)$ [18]. We also assume that the salt dynamics are not affected by the diffusiophoresis of the macromolecules (as usually assumed in diffusiophoresis calculations, cf [4]).

The geometry is symmetric with respect to $x = 0$ and boundary conditions are $\frac{\partial}{\partial x}C_s|_{x=0} = \frac{\partial}{\partial x}C_s|_{x=\pm h/2} = 0$. The 'initial' condition for C_s depends on the experimental situation considered, i.e. salt added to the coflowing water ('spreading' configuration) or salt added to the colloidal solution ('focus' configuration).

Now the above equation can be simplified due to a separation of scales. First, the thickness y_0 of the channel in the y-direction is substantially smaller than its width h ($y_0/h \sim 0.1$) and the salt has diffused along y over the whole thickness y_0 after a distance of the order $z_e \approx U(y_0/2)^2/2D_s \sim 0.6\,\mathrm{mm}$. For larger distances one may accordingly neglect the y dependence of the salt concentration C_s for $z > z_e$ from the inlet, $C_s = C_s(x, z)$.

Equation (6) thus reduces to [20]

$$U\frac{\partial}{\partial z}C_s(x, z) = D_s\frac{\partial^2}{\partial x^2}C_s(x, z). \tag{7}$$

Note that the concentration variations along the flow direction z are much weaker than along x (since $h \ll \ell_s \sim Uh^2/D_s$) and one may neglect the term $\partial^2/\partial z^2$ as compared to $\partial^2/\partial x^2$.

Let us now turn to the solution of this equation. We shall discuss the solution in the 'spreading' case only, while the solution in the 'focus' case can be obtained by symmetry with respect to $x = \pm h/4$ (for $x > 0$ and $x < 0$). The solution to equation (7) with the above boundary conditions can be obtained using the method of images. For the spreading case with the initial condition $C_s(x, z = 0) = C_s^0\Pi_+(x)$ where $\Pi_+(x) = 1 - \Theta(|x| - h/4)$ and $\Theta(x)$ the Heaviside function, this solution reads:

$$C_s(x, z) = C_b + \frac{C_s^0}{2}\sum_{k=-\infty}^{+\infty}\mathrm{Erf}\left[\frac{2x - (h/2) + 2kh}{2\sqrt{\frac{D_s z}{U}}}\right] - \frac{C_s^0}{2}\sum_{k=-\infty}^{+\infty}\mathrm{Erf}\left[\frac{2x - (3/2)h + 2kh}{2\sqrt{\frac{D_s z}{U}}}\right], \tag{8}$$

with C_b the buffer concentration and $\mathrm{Erf}(x) = \frac{2}{\sqrt{\pi}}\int_0^x \mathrm{d}u\ \exp(-u^2)$.

In the large z limit, the salt concentration relaxes to a homogeneous profile. This occurs for distances of the order of the salt mixing length ℓ_s introduced above, typically in the tens of millimeters range.

3.3. Governing equations for the evolution of the colloid profile and a preaveraging approximation

We first consider the dynamic evolution of the colloid profile. Colloids undergo a diffusiophoretic drift V_{DP} under the salt gradient ∇C_s, according to equation (2). In the present geometry, ∇C_s points mainly in the x direction, and so does V_{DP}. Neglecting the diffusion of colloids, the colloid concentration ρ then obeys a convective equation in the form:

$$v_z(y)\frac{\partial\rho}{\partial z}(x, y, z) + \frac{\partial}{\partial x}\left[V_{DP}(x, z)\rho(x, y, z)\right] = 0, \tag{9}$$

with $v_z(y) = \frac{3}{2}U(1 - (\frac{2y}{y_0})^2)$ the parabolic velocity profile within the channel thickness.

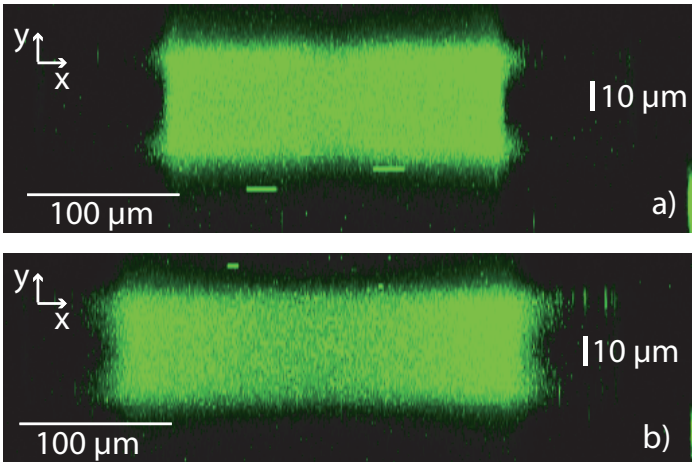

Figure 6. Confocal imaging of the colloidal solution in the x, y plane, for a constant distance z from the channel inlet: (a) $z = 0.7$ cm and (b) $z = 8$ cm. The images are taken in the spreading situation (with 10 mM of LiCl). These images show that the colloidal solution is mainly uniform in the y-direction within the thickness of the channel.

In the experimental setup, the measured density profiles are obtained by y-averaging the fluorescence intensity over an optical window whose size is set by the depth of field of the objective. The quantity of interest is therefore the averaged density profile $\bar{\rho}(x, z) \equiv \langle \rho(x, y, z) \rangle$, where $\langle \cdot \rangle$ stands for an average over the optical window along the y-axis:

$$\langle \cdot \rangle = \int \mathrm{d}y (\cdot) \mathcal{O}(y) \tag{10}$$

with $\mathcal{O}(y) = \mathcal{O}_0 (\frac{\sin(u/4)}{u/4})^2$ the intensity distribution along the optical axis, and $u = \frac{2\pi}{\lambda} NA^2 \tilde{y}$, $\tilde{y}$ the distance along y-axis to the focus plane [21]; $\lambda = 510$ nm is the average wavelength of the illumination source, NA the numerical aperture of the objective (here, NA $= 0.3$); $\mathcal{O}_0$ the normalizing factor such that $\int \mathrm{d}y\, \mathcal{O}(y) = 1$. By averaging equation (9) over the optical window, one obtains the following dynamical equation for the colloid density:

$$U \frac{\partial}{\partial z} \left\langle \frac{3}{2} \left[1 - (2y/y_0)^2 \right] \rho(x, y, z) \right\rangle + \frac{\partial}{\partial x} \left[V_{\mathrm{DP}}(x, z) \bar{\rho} \right] = 0, \tag{11}$$

where $\bar{\rho}(x, z) \equiv \langle \rho(x, y, z) \rangle$ is the measured colloid profile.

To proceed further we perform a 'decoupling approximation', assuming

$$\left\langle \frac{3}{2} \left(1 - \left(\frac{2y}{y_0} \right)^2 \right) \rho(x, y, z) \right\rangle \simeq \left\langle \frac{3}{2} \left(1 - \left(\frac{2y}{y_0} \right)^2 \right) \right\rangle \bar{\rho}(x, z). \tag{12}$$

Such an approximation is justified for an approximately constant colloidal profile over the channel's thickness. This is indeed a good approximation as shown by a scanning confocal imaging of the colloidal profile in figure 6: the fluorescence intensity is roughly constant over the channel width, even if a slight variation is observed in both cases near the walls due to the reduced velocity of the fluid near the wall in the Poiseuille flow. This does assess the validity of the decoupling approximation.

One may thus deduce a closed equation for the averaged density profile $\bar{\rho}$:

$$U\frac{\partial\bar{\rho}}{\partial z}(x,z)+\frac{\partial}{\partial x}\left[\tilde{V}_{\rm DP}(x,z)\bar{\rho}\right]=0, \tag{13}$$

where we introduced the renormalized diffusiophoretic velocity $\tilde{V}_{\rm DP}$ taking into account the Poiseuille velocity profile within the channel thickness, defined as

$$\begin{aligned}\tilde{V}_{\rm DP}&=\alpha_{\rm Pois}V_{\rm DP},\\ \alpha_{\rm Pois}&=\left\langle\frac{3}{2}\left[1-(2y/y_0)^2\right]\right\rangle^{-1}.\end{aligned} \tag{14}$$

For the present experimental situation and parameters, the numerical evaluation of the Poiseuille correction $\alpha_{\rm Pois}$ gives $\alpha_{\rm Pois}\simeq 1.9$.

We thus conclude that averaging along y over the channel thickness y_0 slightly renormalizes the diffusiophoretic mobility as $\tilde{D}_{\rm DP}=\alpha_{\rm Pois}D_{\rm DP}$, with $D_{\rm DP}$ given in equation (3).

3.4. Colloid drift, effective diffusion and saturation

On this basis, one may thus derive the effective diffusive behavior of the colloids. We start with a qualitative argument. The growth rate for the width of the colloidal solution is:

$$\frac{{\rm d}w}{{\rm d}t}=2\tilde{V}_{\rm DP}=2\tilde{D}_{\rm DP}\nabla\log C_{\rm s}. \tag{15}$$

The gradient of the salt concentration occurs over a distance $\delta\approx\sqrt{D_{\rm s}t}$ (with $t=z/U$), so that

$$\frac{{\rm d}w}{{\rm d}t}\approx\pm\frac{\tilde{D}_{\rm DP}}{\sqrt{D_{\rm s}t}} \tag{16}$$

with the sign depending on the direction of the salt gradient. One thus concludes

$$w(t)=w(0)\pm\sqrt{2D_{\rm eff}t} \tag{17}$$

with the effective diffusion coefficient scaling as $D_{\rm eff}\sim\tilde{D}_{\rm DP}^2/D_{\rm s}$.

This argument can be developed more systematically. Applying the method of characteristics to equation (13), one deduces that the position of the interface $x=X(z)$ between the colloidal solution and the co-flowing water obeys the simple differential equation:

$$\frac{{\rm d}X}{{\rm d}z}=\frac{\tilde{V}_{\rm DP}(X(z),z)}{U}, \tag{18}$$

together with the initial condition $X(0)=\pm\frac{h}{4}$ (the interface position at the channel inlet). We recall that in this equation, $\tilde{V}_{\rm DP}=\tilde{D}_{\rm DP}\nabla\log C_{\rm s}$, with $\tilde{D}_{\rm DP}=\alpha_{\rm Pois}D_{\rm DP}$ and $D_{\rm DP}$ given in equation (3).

Let us first focus on the behavior of the interface at small timescales: for small z, the salt concentration profile reduces to the first term ($k=0$) in equation (8), corresponding to diffusion of a initial step concentration. Accordingly, the change in position of this interface, $x(z/U)\equiv X(z/U)-X(0)$ obeys the simple differential equation:

$$\frac{{\rm d}x}{{\rm d}t}=\tilde{V}_{\rm DP}\simeq\tilde{D}_{\rm DP}\frac{(C_{\rm s}^0/2\sqrt{\pi D_{\rm s}t})\,\exp\left(-x^2/4D_{\rm s}t\right)}{C_{\rm b}+(C_{\rm s}^0/2)\left[1+{\rm Erf}\left(x/2\sqrt{D_{\rm s}t}\right)\right]} \tag{19}$$

with $t = z/U$ and C_b the buffer concentration. Note that we assume that the presence of the buffer does not modify this expression—which has been obtained in principle for a binary electrolyte—an assumption that is valid for low buffer concentration.

This equation has a solution in the form $x(t) = \gamma\sqrt{D_s t}$, where the coefficient γ verifies the implicit equation:

$$\gamma = \frac{1}{\sqrt{\pi}} \frac{\tilde{D}_{DP}}{D_s} \frac{\exp[-\gamma^2/4]}{\epsilon + \frac{1}{2}\left[1 + \mathrm{Erf}\,(\gamma/2)\right]}, \tag{20}$$

with $\epsilon = C_b/C_s^0$ the ratio of the buffer to salt concentration. The width of the colloidal solution $w(z)$ can be written accordingly $w(z) = w(0) \pm 2\gamma\sqrt{D_s \frac{z}{U}}$, so that the effective diffusion coefficient D_{eff}, defined as

$$w(z) = w(0) \pm \sqrt{2 D_{eff} \frac{z}{U}}, \tag{21}$$

is related to γ according to

$$D_{eff} = 2 D_s \gamma^2. \tag{22}$$

Typically, $\tilde{D}_{DP}/D_s \sim 0.1$, so that a small γ expansion of the right-hand side of equation (20) can be conducted. To first order in $\tilde{D}_{DP}/D_s$, this yields the following expression for γ:

$$\gamma = \frac{2}{\sqrt{\pi}} \frac{\tilde{D}_{DP}}{D_s} (1+2\epsilon)^{-1} \left[1 + \frac{2}{\pi} \frac{\tilde{D}_{DP}}{D_s} (1+2\epsilon)^{-2}\right]^{-1} \tag{23}$$

with $\epsilon = C_b/C_s^0$ and C_s^0 and C_b the salt and buffer concentrations.

Gathering the previous results, one obtains the following expression for the effective diffusion coefficient D_{eff}:

$$D_{eff} = \frac{8}{\pi} \frac{\tilde{D}_{DP}^2}{D_s} \left[1 + 2\epsilon + \frac{2}{\pi(1+2\epsilon)} \frac{\tilde{D}_{DP}}{D_s}\right]^{-2}. \tag{24}$$

At long distances z, the salt solution becomes homogeneous and $V_{DP} \to 0$. This is expected to occur when the salt has diffused over the (half) width of the channel: $z_\infty \approx U(h/2)^2/2D_s$. This gives $w_\infty - w_0 \approx \frac{h}{2}\sqrt{\frac{D_{eff}}{D_s}} \approx w_0\sqrt{\frac{D_{eff}}{D_s}}$. We have checked this result by solving equation (18) numerically using Mathematica©. Quantitatively one finds that the saturating value for the colloid width Δw_∞ is given as:

$$\Delta w_\infty = A_\infty w_0 \sqrt{\frac{D_{eff}}{D_s}}, \tag{25}$$

with $A_\infty \simeq 0.63$ a numerical constant.

3.5. Comparison with experiments

The main results of the previous section, summarized in equations (21), (24) and (25), are now compared to the experimental data.

We start by comparing in figure 3 the effective diffusion coefficient to the prediction in equation (24). To this end we have measured independently the value of the zeta potential of

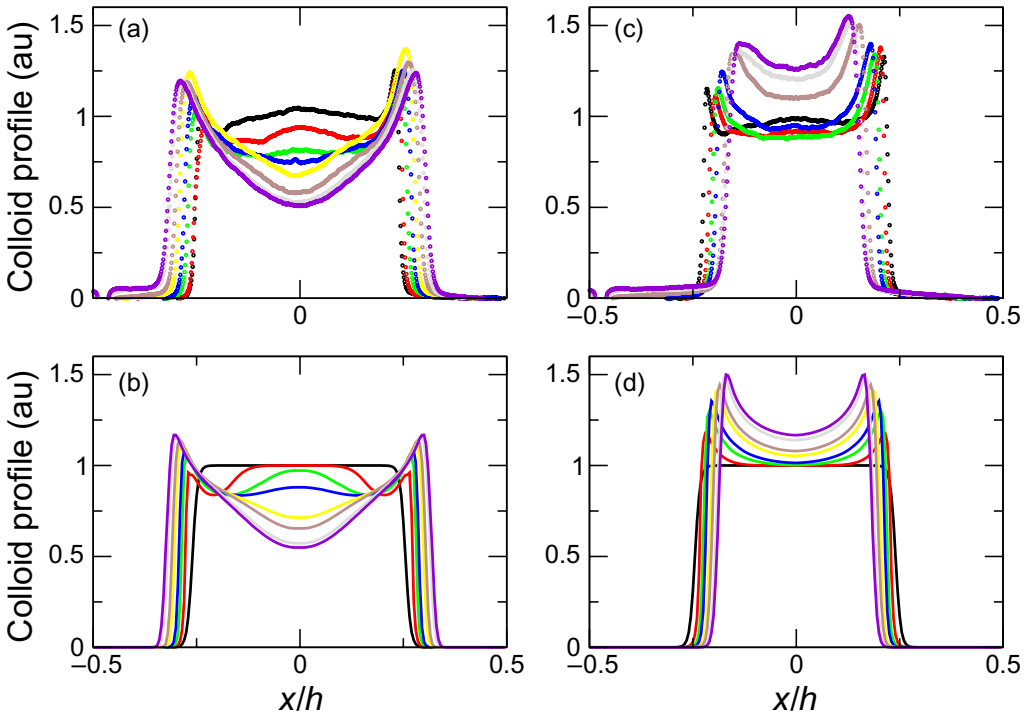

Figure 7. Evolution of the fluorescence profiles for 10 mM of LiCl. Experimental profiles for the spreading (a) and focusing (c) configurations are compared to theoretical profiles (b) and (d) obtained as detailed in section 3.6.

the colloids in the buffer solution, $\zeta = -35$ mV (see appendix for details). Using this value, the agreement between the theory and our experiment is seen to be excellent, provided the value of α_{Pois} is set to 1.8, i.e. slightly smaller than the theoretical value obtained above ($\alpha_{\mathrm{Pois}} = 1.9$).

Secondly, in figure 5, we compare the experimental results for Δw_∞ with the theoretical predictions obtained in equation (25) for the dependence on the salt diffusive coefficient and salt concentration (via the dependence on ϵ in equation (25)). Note that this comparison is free of any parameter.

Thirdly, in figure 4 we compare the complete dynamical evolution of the width $\Delta w(z)$ versus the effective time $t = z/U$ with the theoretical prediction obtained by solving equation (18) numerically. Again, the agreement between the theory and our experiment is excellent, without any free parameter. Note that the transition between the 'diffusive' and stationary regimes occurs when the salt has diffused over the channel width, here $z/U \approx (h/2)^2/2D_s \simeq 14$ s, so that $(z/U)^{1/2} \simeq 3.7\,\mathrm{s}^{1/2}$: this is indeed consistent with the experimental results.

Altogether excellent agreement is found between the theory and experimental results.

3.6. Numerical resolution of the density profiles

The above comparison can be extended to the detailed colloid profiles. Experimental profiles are exhibited in figures 7(a)–(c), denoting a rather complex shape: the colloid density is maximum at the edges of the fluorescent band, while colloids are depleted from the center of the microchannel both in the 'spreading' configuration and in the focusing configuration (even if the

effect is less pronounced in the latter case). This depletion occurs in the center of the channel, i.e. where the salt concentration is the smallest (figures 7(a) and (b)). The origin of this counter-intuitive effect lies in the specific form of the solute-induced driving force, which is proportional to the gradient of the *logarithm* of the salt concentration, $V_{DP} \propto \nabla \log C_s$ (i.e. proportional to the gradient of chemical potential). The velocity of colloids is accordingly *largest* in the region where the salt concentration goes to zero ($C_s \to 0$). Colloids are therefore depleted from this part of the system and accumulate close to the interface. In the 'focusing' situation the effect is less pronounced since the salt-poor region is free of colloids.

On the theoretical side, the density profile can be predicted from the convective equation discussed above, equation (13). To solve this equation, we have simulated—from a Lagrangian point of view—the dynamical evolution of particles, which are distributed initially over the channel:

$$U\frac{\mathrm{d}X}{\mathrm{d}z} = \tilde{V}_{DP}(X(z), z), \tag{26}$$

with $X(z=0) = X_i$ the initial position of particle i, $\tilde{V}_{DP} = \alpha_{Pois} V_{DP}$ and V_{DP} given in equation (2). The numbers of particle i are distributed over the channel according to the initial distribution.

For a given salt and ζ-potential of the particle, the diffusiophoretic mobility D_{DP} is given by equation (3), while the salt concentration profile is given in equation (8). Equation (26) is then solved using a simple Euler scheme for the various initial position X_i and the density profile at a given time z/U and position x is determined by the number of particles per unit length ending at this position x. In practice, we discretized the channel width h in small intervals Δx ($\Delta x/h = 1/200$) and counted the number of particles within a given interval $x \pm \frac{\Delta x}{2}$.

As a further refinement, we took into account the measured distribution in ζ potential of the particles. This ingredient is not essential to reproduce the experimental profiles, but it does smooth out the predicted profiles (by allowing for a distribution of particle velocities). Indeed the measurements of the zeta potential of the colloidal particles used in this study lead to a value $\zeta = -35$ mV with a distribution of zeta potential typically of ± 5 mV. We have modeled this behavior by assuming a Gaussian distribution of zeta potential with a half-width 5 mV, and averaged with the corresponding weight the density profiles obtained for the different values of ζ. Results for the density profiles obtained using this procedure are shown in figures 7(b) and (d).

We quote finally that we also solved directly the convection equation, equation (13), using a classical Lax–Friedrich numerical scheme, which provided very similar results. The Lax–Friedrich scheme, however, introduces a small numerical diffusion, which is avoided in the previous approach.

The comparison between these simulations and the actual fluorescence profiles is again excellent and all the detailed features of the experimental profiles are reproduced by the simulation.

4. Application to microfluidics

By providing a means to set up a controlled salt gradient, microfluidics techniques have enabled us to provide a thorough description of diffusiophoresis and to compare in great detail theory and experiments. In turn, we discuss in this section how diffusiophoresis could be used to provide

functionalities to lab-on-a-chip devices. First of all, we emphasize that the present mechanism can be seen as the transduction of chemical energy into directional movement of otherwise slowly moving species. As compared to other driving mechanisms (such as electrophoresis, thermophoresis, acoustic wave or electrowetting) diffusiophoresis does not require the input of external energy, the internal energy being here the gradient of salt chemical potential. In the perspective of its use for lab-on-a-chip applications, being able to circumvent the use of (for example) a high-voltage generator is an important advantage. In the following paragraphs, we describe several applications which could be implemented using the phenomenon described previously.

4.1. Hydrophoretic focusing

First, focusing an assembly of particles is necessary in a wide range of miniaturized devices. For example, high-throughput flow cytometry [22] can detect minute quantities of a target reagent as soon as the sample is confined in a sufficiently small volume. Focusing can also be utilized to reach small timescale in order to assess rapid events [23]. In these respects, hydrodynamic focusing has been widely used so far along with other strategies such as electrokinetic focusing [24]. Hydrodynamic focusing consists in creating a stream which encases the sample stream, thus reducing its width. In our experimental configuration, this can be achieved by applying a higher flow rate to the side streams than to the central one. The final width of the colloidal solution is then predicted to be [25]:

$$w_\infty^{\text{hydro}} = w_0 \frac{3}{1+2r}. \tag{27}$$

where r is the ratio between the speed of injection of the central stream and the side one.

Now, by adding a small quantity of salt to the colloidal solution, it is possible to increase this effect significantly using diffusiophoretic migration. This combined focusing effect is demonstrated in figure 8. As the hydrofocusing width establishes quickly in the inlet region, it decouples from diffusiophoresis. The hydrofocused jet with width w_∞^{hydro} serves as an initial configuration to which the diffusiophoretic mechanism further applies. The analysis for the diffusiophoretic focusing can thus be applied and predicts that:

$$w_\infty^{\text{hydro+diffusio}} = w_\infty^{\text{hydro}} \left(1 - A_\infty \sqrt{\frac{D_{\text{eff}}}{D_{\text{s}}}}\right). \tag{28}$$

Altogether one thus deduces that

$$w_\infty = w_0 \frac{3}{1+2r} \left(1 - A_\infty \sqrt{\frac{D_{\text{eff}}}{D_{\text{s}}}}\right). \tag{29}$$

This expression is compared to the experimental results measured for different values of r and the agreement is excellent, again without any free parameter. For a salt concentration of 20 mM of LiCl, the increase in focusing reaches 40%.

4.2. Concentration

One of the basic operations needed in lab-on-chip device is extraction of particles from an initially concentrated solution. This can be seen as the counterpart of centrifugation in classical

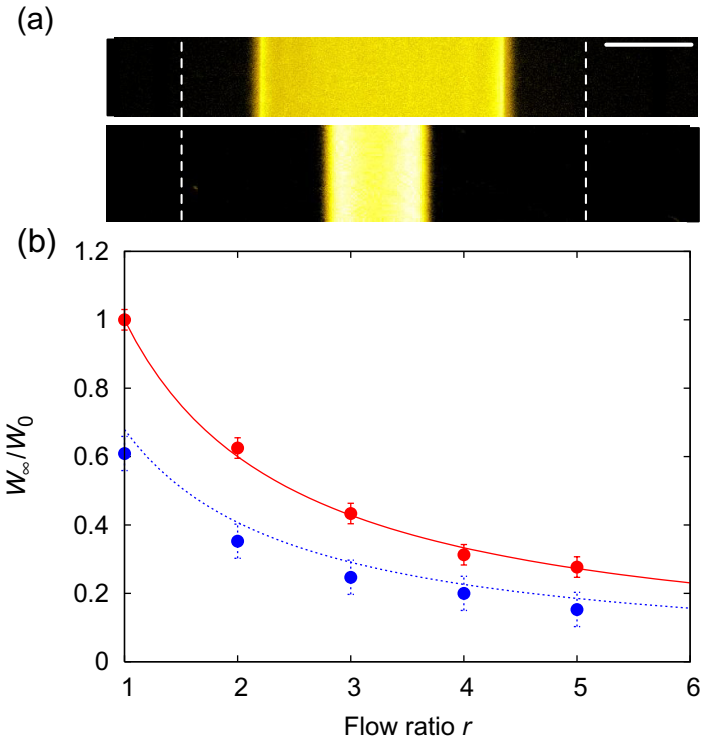

Figure 8. A colloidal solution is injected into the central inlet at a mean velocity U, whereas the coflowing buffer is injected at a mean velocity $r \times U$. Top: colloid density profile for $r = 2$, far from the inlet: (a), no salt is added to any of the inlets; (b) 20 mM LiCl is added only to the colloidal solution. The vertical dashed lines indicate the initial width of the colloidal solution (at the inlet). The scale bar is 50 μm. Bottom: saturating width of the colloidal solution, w_∞, normalized by its initial value w_0 as a function of the flow ratio r, without salt (red circles) and with salt (blue circles) added to the colloidal solution. Dashed lines are theoretical predictions based on the hydrodynamic focusing mechanism alone and in conjunction with the diffusiophoretic focusing (bottom).

laboratory operations. An efficient concentration process can be realized using diffusiophoresis. Starting from an homogeneous solution of colloidal particles, adding a small amount of salt induces a separation of the colloids, as shown in figure 9 where the same colloidal solution is injected in both channels while a small quantity of salt is added to one of the solutions. By this means, the colloids move towards the higher salt concentration regions. Moreover, solving numerically the equation of motion of the colloids using these new initial conditions, provides profiles which show excellent agreement with the experimental profiles, see figure 9.

4.3. Separation of colloids

Another basic operation that can be achieved by diffusiophoresis is the separation of colloids bearing different surface charges which are initially present in the same solution. The extent of the diffusiophoretic drift depends on the ζ potential of the particles both through the chemiphoretic contribution and through the electrophoresis of the particles in the field created by

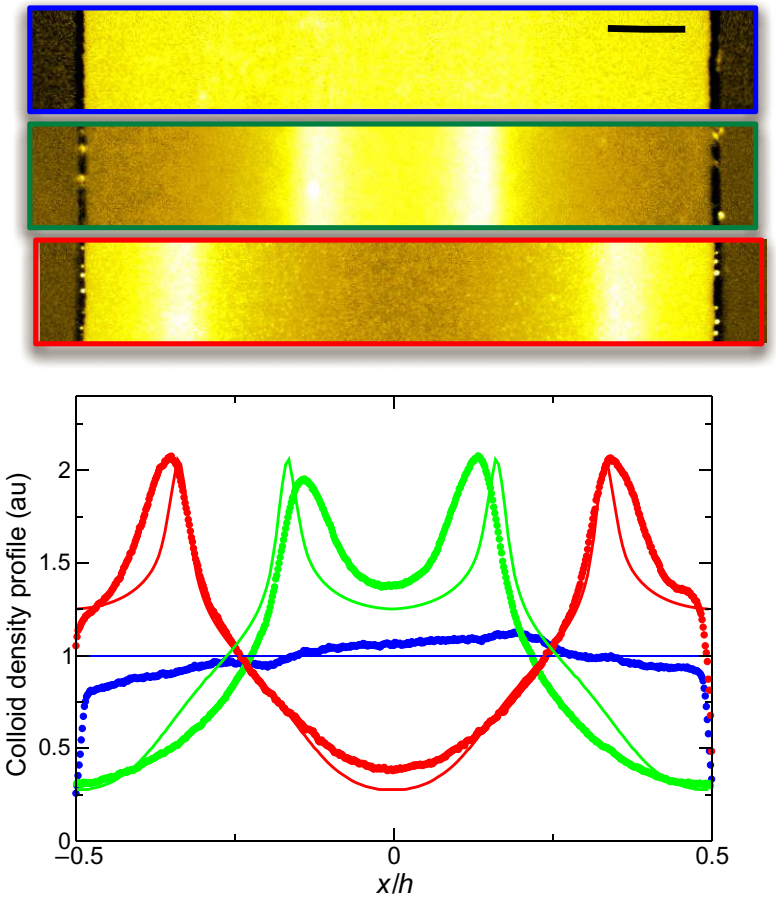

Figure 9. A homogeneous colloidal solution is injected in all the channels of the microfluidic device: salt (50 mM of LiCl) is added to (a) all the channels, (b) only the central inlet, (c) only the side inlets. Top: fluorescence images acquired at $z = 80$ mm from the inlet. The scale bar is 50 μm. Bottom: experimental fluorescence profiles for the three situations as compared to the theoretical predictions.

the differential diffusion of the anion and the cation. Hence, particles bearing different surface charges would migrate differently under the same salt gradient. As a proof of principle of this concept, two different types of particles were mixed in the same buffer solution and injected in the microfluidic device. Amine modified silica colloids having a smaller ζ potential (-25 mV as measured by a zeta sizer) are seen to migrate to a smaller extent as compared to the native silica colloids, see figure 10. Adsorption of amine-modified particles on the glass slide of the channel is visible both in the pictures and in the shape of the fluorescence profile. This may be explained by the weaker electrostatic repulsion between the glass slide (negatively charged at this pH) and the particles. Because of this adsorption the soft peaks indicating accumulation of particles at the salt/colloid interface are not visible in this case. However, the difference of behavior between the two sorts of particles is clearly visible. By placing an outlet to the channel at $x/h \simeq 0.25$, one may in principle perform a quantitative enrichment of the solution in native silica colloids as compared to the original solution.

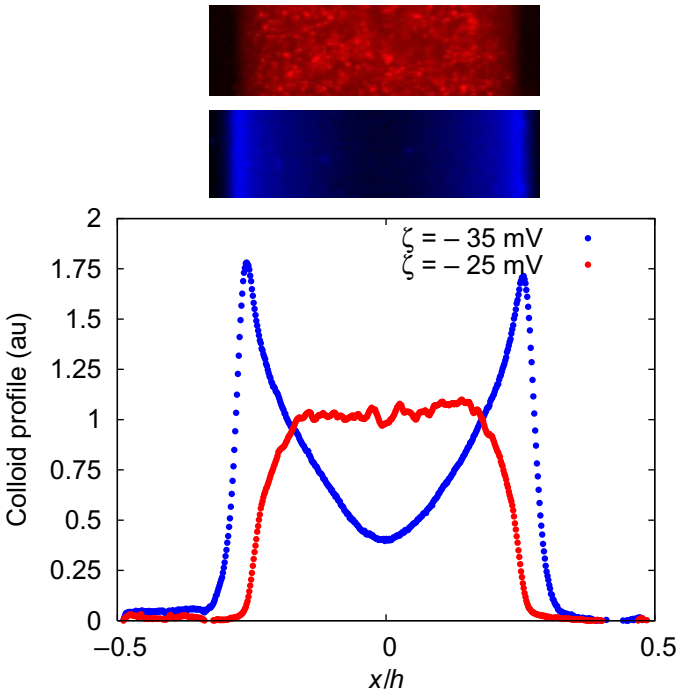

Figure 10. Colloid separation experiment. In the same solution, two types of particles with different zeta potential are mixed. In red, particles functionalized with amine ($\zeta \simeq -25\,\mathrm{mV}$). In blue, native silica particles ($\zeta \simeq -35\,\mathrm{mV}$). The profiles are acquired at $z/U = 10\,\mathrm{s}$ from the inlet.

5. Conclusion

We have shown that the migration of slowly diffusing colloids can be enhanced and controlled by diffusiophoresis. Setting-up a controlled salt gradient in a microfluidic chip, both spreading and focusing of an assembly of particles were achieved with an effective diffusion coefficient two orders of magnitude larger than the bare Brownian diffusion coefficient of the particles.

Quantitative agreement with theory was obtained—with only experimentally measurable input parameters—on the dependance of the phenomenon's amplitude with the salt and on the precise shape of the colloid concentration profiles. We have also provided proofs of principle for several basic operations, such as hydrophoretic focusing, concentration and sorting of particles showing the potential relevance of diffusiophoresis in the framework of lab-on-a-chip applications. Current and future work could deal with the application of diffusiophoresis to biological macromolecules (preliminary experiments confirm the applicability of diffusiophoretic manipulation of DNA molecules). If silica colloids provide an excellent model system, rationalization of the movement of more complex systems, in terms of structure and surface chemistry for example, under controlled salt gradient remains an important issue.

Acknowledgments

We thank J Bellier and P Joseph for fruitful interactions, the CTμ for the confocal images, S Roux for his help in the zeta potential measurements and the INL microfabrication center.

LB acknowledges support from the von Humboldt foundation. This work was supported by ANR program pNANO.

Appendix. Experimental methods

A.1. Experimental setup and fabrication of the microchannels

To study the diffusiophoretic migration of fluorescent colloids we have considered Ψ-shaped microfluidic devices that present three inlets (figure 1). The devices are fabricated using standard soft photolithography techniques. A SU8 master mold of 35 μm thick is produced by UV photolithography on a silicon wafer. The width of the channel (h) is set to 400 μm. A mixture of polydimethylsiloxane (PDMS) and crosslinker is then poured onto the mold and baked for 3 h at 70 °C. The bottom of the channels are then sealed with a glass slide bonded to the PDMS by a oxygen plasma. Unless otherwise stated the solutions (colloidal, buffer or salt solutions) in all the inlets have the same velocity $U = 5.95\,\mathrm{mm\,s^{-1}}$.

A.2. Preparation of the solutions

All the solutions are prepared using deionized water of resistivity 18.2 MΩ cm from a Milli-Q purification system (Millipore, USA). The solutions are all buffered. The buffer solution (1 mM of TRIS HCl, pH 9) is prepared by weighting adapted amount of TRIS–HCl (Sigma Aldrich) and adding NaOH (100 mM solution) towards the desired pH. The colloidal solutions are composed of silica colloids (Kisker, Germany, 200 nm in diameter) labeled with FITC fluorescent probe at a volume fraction of 0.005% in the buffer solution. Unless otherwise stated, the surface state of the particle is native but amine-coated particles are used in certain circumstances (see section 4.3). We gently sonicate the colloidal solution for a few minutes just before use to avoid undesirable aggregation during observation. We have considered different salt solutions: LiCl, NaCl and KCl (also Sigma Aldrich) at different concentrations ranging from 5 to 50 mM. They were all prepared in the buffer solution.

A.3. Epi-fluorescence microscopy

The colloid concentration profiles are imaged at different positions along the z-axis of the microfluidic channel by using an inverted optical microscope (Eclipse, Nikon) and a 10× objective. A UV–visible source illuminates the sample through the objective and the fluorescence intensity is collected by a CCD camera (Orca AG, Hamamatsu). For each z-position, the focus is made at the bottom of the microfluidic channel and a 1344 × 1024 16-bit TIFF-image is recorded. Typical acquisition time is 3 s.

A.4. Image treatment

All the fluorescent pictures, as those presented on figure 1, were processed (background subtraction, contrast enhancement and LUT change) using ImageJ. All other image treatment routines were written in Python using the Python Image Library. For a given picture, averaging the fluorescence intensity over z-lines yields the transverse fluorescence profile. The transverse coordinate x is normalized by the width h of the microchannel, and the origin is set at the middle of the channel. To normalize the fluorescence intensity, we first subtract the background

intensity and then rescale the intensity so that the initial top-hat profile reaches the value 1 at the entrance ($z = 0$) of the microfluidic channel. The width of the colloidal profile $w(z)$ at a given position z is then defined as the width where the normalized profile is equal to 0.5. The width of the colloidal profile at the entrance of the channel ($z = 0$) is called w_0.

A.5. Confocal microscopy

In order to determine colloidal concentration profiles along the y-axis, we perform confocal scanning microscopy using an LSM 510 META confocal microscope (Zeiss) and a 50× (NA 0.85) epiplan/neofluar objective. A 2D map of the colloidal concentration is determined in the x–y plane for several z-positions.

A.6. Particle characterization

The ζ potential of the particles were measured using a Zetasizer nano (Malvern). The colloids were diluted in the buffer solution at a concentration of 0.0005% and the measurement was carried using the custom commercial software provided by Malvern. For better reproducibility, we used a measurement mode considering a monodisperse assembly of particles. Averaging over 10 measurements yields ζ-potential of -35 ± 5 mV. We also checked the actual size of the particles by dynamic light scattering using the same apparatus. This confirmed the value given by the manufacturer (200 nm in radius).

References

[1] Squires T M and Quake S R 2005 Microfluidics: fluid physics at the nanoliter scale *Rev. Mod. Phys.* **77** 977–1026
[2] Stone H A, Stroock A D and Ajdari A 2004 Engineering flows in small devices: microfluidics toward a lab-on-a-chip *Annu. Rev. Fluid Mech.* **36** 381–411
[3] Derjaguin B V, Sidorenkov G P, Zubashchenkov E A and Kiseleva E V 1947 Kinetic phenomena in boundary films of liquids *Kolloidn. Zh.* **9** 335–47
[4] Anderson J L 1989 Colloid transport by interfacial forces *Annu. Rev. Fluid Mech.* **21** 61–99
[5] Velev O D and Bhatt K H 2006 On-chip micromanipulation and assembly of colloidal particles by electric fields *Soft Matter* **2** 738–50
[6] Braun D and Libchaber A 2002 Trapping of DNA by thermophoretic depletion and convection *Phys. Rev. Lett.* **89** 188103
[7] Duhr S and Braun D 2006 Why molecules move along a temperature gradient *Proc. Natl Acad. Sci. USA* **103** 19678–82
[8] Weinert F M and Braun D 2008 Observation of slip flow in thermophoresis *Phys. Rev. Lett.* **101** 168301
[9] Piazza R 2008 Thermophoresis: moving particles with thermal gradients *Soft Matter* **4** 1740–4
[10] Anderson J L and Prieve D C 1991 Diffusiophoresis caused by gradients of strongly adsorbing solutes *Langmuir* **7** 403–6
[11] Ebel J P, Anderson J L and Prieve D C 1988 Diffusiophoresis of latex-particles in electrolyte gradients *Langmuir* **4** 396–406
[12] Prieve D C and Roman R 1987 Diffusiophoresis of a rigid sphere through a viscous electrolyte solution *J. Chem. Soc. Faraday Trans.* II **83** 1287–306
[13] Staffeld P O and Quinn J A 1989 Diffusion-induced banding of colloid particles via diffusiophoresis. 1. Electrolytes *J. Colloid Interf. Sci.* **130** 69–87

[14] Staffeld P O and Quinn J A 1989 Diffusion-induced banding of colloid particles via diffusiophoresis. 2. Non-electrolytes *J. Colloid Interf. Sci.* **130** 88–100
[15] Kim M J and Breuer K S 2007 Controlled mixing in microfluidic systems using bacterial chemotaxis *Anal. Chem.* **79** 955–9
[16] Abécassis B, Cottin-Bizonne C, Ybert C, Ajdari A and Bocquet L 2008 Boosting migration of large particles by solute contrasts *Nat. Mater.* **7** 785–9
[17] Hunter R J 1991 *Foundations of Colloid Science* (New York: Oxford University Press)
[18] Josserand J, Lagger G, Jensen H, Ferrigno R and Girault H H 2003 Contact galvanic potential differences at liquid vertical bar liquid interfaces—part II. Contact diffusion potentials in microsystems *J. Electroanal. Chem.* **546** 1–13
[19] Munson M S, Cabrera C R and Yager P 2002 Passive electrophoresis in microchannels using liquid junction potentials *Electrophoresis* **23** 2642–52
[20] Salmon J B and Ajdari A 2007 Transverse transport of solutes between co-flowing pressure-driven streams for microfluidic studies of diffusion/reaction processes *J. Appl. Phys.* **101** 074902
[21] Meinhart C D, Wereley S T and Gray M H B 2000 Volume illumination for two-dimensional particle image velocimetry *Meas. Sci. Technol.* **11** 809–14
[22] Nolan J P and Sklar L A 1998 The emergence of flow cytometry for sensitive, real-time measurements of molecular interactions *Nat. Biotechnol.* **16** 633–8
[23] Knight J B, Vishwanath A, Brody J P and Austin R H 1998 Hydrodynamic focusing on a silicon chip: mixing nanoliters in microseconds *Phys. Rev. Lett.* **80** 3863–6
[24] Schrum D P, Culbertson C T, Jacobson S C and Ramsey J M 1999 Microchip flow cytometry using electrokinetic focusing *Anal. Chem.* **71** 4173–7
[25] Lee G B, Chang C C, Huang S B and Yang R J 2006 The hydrodynamic focusing effect inside rectangular microchannels *J. Micromech. Microeng.* **16** 1024–32